

High-Performance Fine Defect Detection in Artificial Leather Using Dual Feature Pool Object Detection

Lin Huang^{a,c}, Weisheng Li^{a,*}, Linlin Shen^b, Xue Xiao^c, Suihan Xiao^d

^a*Chongqing University of Posts and Telecommunications, No.2, Chongwen Road, Nan'an District, Chongqing, 400065, China*

^b*Shenzhen University, No.3688 Nanshan Avenue, Nanshan District, Shenzhen, 518061, China*

^c*Inspur Industrial Internet Co., Ltd, No.1036 Langchao Road, Lixia District, Jinan, Shandong, 250101, China*

^d*Chongqing Zhenyuan Innovation Technology Co., Ltd, No. 988, Haier Road, Jiangbei District, Chongqing, 400026, China*

Abstract

In this study, the structural problems of the YOLOv5 model were analyzed emphatically. Based on the characteristics of fine defects in artificial leather, four innovative structures, namely DFP, IFF, AMP, and EOS, were designed. These advancements led to the proposal of a high-performance artificial leather fine defect detection model named YOLOD. YOLOD demonstrated outstanding performance on the artificial leather defect dataset, achieving an impressive increase of 11.7% - 13.5% in AP_{50} compared to YOLOv5, along with a significant reduction of 5.2% - 7.2% in the error detection rate. Moreover, YOLOD also exhibited remarkable performance on the general MS-COCO dataset, with an increase of 0.4% - 2.6% in AP compared to YOLOv5, and a rise of 2.5% - 4.1% in AP_S compared to YOLOv5. These results demonstrate the superiority of YOLOD in both artificial leather defect detection and general object detection tasks, making it a highly efficient and effective model for real-world applications.

Keywords:

Object detection, Defect detection, Artificial leather, Fine defect

*Corresponding Author

Email addresses: h72001346@163.com (Lin Huang), liws@cqupt.edu.cn (Weisheng Li), llshen@szu.edu.cn (Linlin Shen), xiaoxue@inspur.com (Xue Xiao), x@zmetacn.com (Suihan Xiao)

1. Introduction

Artificial leather, also known as synthetic leather, has gained widespread popularity in various industries due to its cost-effectiveness and eco-friendly attributes. However, ensuring its quality and identifying fine defects remain significant challenges. Traditional defect detection of artificial leather primarily relies on human eyes, which has several limitations concerning detection efficiency and accuracy. The drawbacks of human visual detection are twofold. Firstly, it cannot meet the demands of long-term and high-speed production lines, as human eyes are susceptible to issues such as fatigue and distraction. Secondly, the evaluation standards for defects by the human eye also exhibit a certain degree of subjectivity, making it difficult to ensure consistent standard. Additionally, there are two challenges in detecting artificial leather using traditional machine vision algorithms(Pourkaramdel et al. (2022)). First, the irregular dermatoglyphics of artificial leather make a big challenge to the accuracy of defect detection. Second, the small size and inconspicuous features of defects make them difficult to be detected, resulting in a high rate of missed inspections and false positives. However, with the rise of deep learning, real-time object detection technology(Redmon et al. (2016); Redmon and Farhadi (2017, 2018); Bochkovskiy et al. (2020); Wang et al. (2021); Glenn (2021); Long et al. (2020); Huang et al. (2021); Chen et al. (2021); Ge et al. (2021); Wang et al. (2022); Lin et al. (2017); Tan et al. (2020); Liu et al. (2019, 2016); Cao et al. (2021); Karaman et al. (2023)) has matured significantly, greatly improving object detection average precision (AP) and detection speed. This progress opens up the possibility of applying deep learning to artificial leather defect detection.

In recent years, object detection algorithms have been primarily categorized into two major research directions: one-stage object detection and two-stage object detection. While two-stage object detection(He et al. (2017); Cai and Vasconcelos (2018); Girshick et al. (2014); Girshick (2015); Ren et al. (2015); Dai et al. (2016); Pang et al. (2019)) outperforms one-stage object detection(Redmon et al. (2016); Redmon and Farhadi (2017, 2018); Bochkovskiy et al. (2020); Wang et al. (2021); Glenn (2021); Long et al. (2020); Huang et al. (2021); Chen et al. (2021); Ge et al. (2021); Wang et al. (2022); Lin et al. (2017); Tan et al. (2020); Liu et al. (2019, 2016)) in terms of average precision (AP), the latter excels in inference speed and is

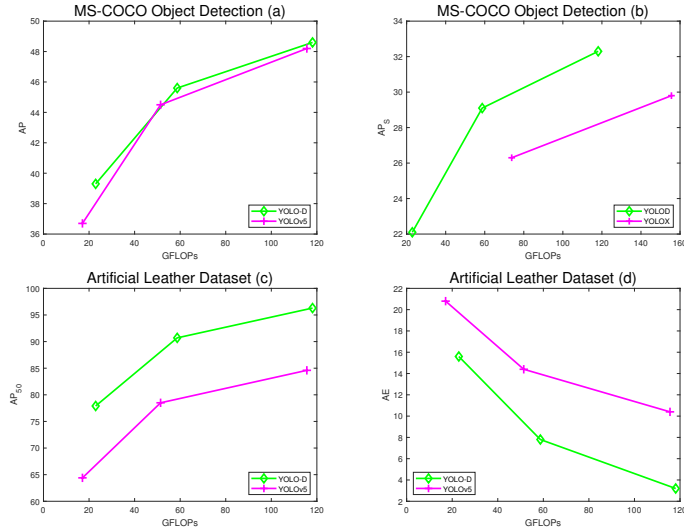


Figure 1: (a) illustrates the comparison of AP on MS-COCO between the proposed YOLOD and YOLOv5. (b) illustrates the comparison of AP_S on MS-COCO between the proposed YOLOD and YOLOX. (c) illustrates the comparison of AP_{50} on ALD between the proposed YOLOD and YOLOv5. (d) illustrates the comparison of AE on ALD between the proposed YOLOD and YOLOv5.

thus highly suitable for real-time applications in various industries. Notably, the YOLO(You Only Look Once) model, along with SSD(Liu et al. (2016)), stands as one of the most representative detectors among the algorithms of one-stage object detection. The YOLO series of algorithms has evolved from version 1 to version 8(Redmon et al. (2016); Redmon and Farhadi (2017, 2018); Bochkovskiy et al. (2020); Wang et al. (2021); Glenn (2021); Long et al. (2020); Huang et al. (2021); Chen et al. (2021); Ge et al. (2021); Wang et al. (2022)), and inspires a number of variants such as pp-YOLOv1(Long et al. (2020)), pp-YOLOv2(Huang et al. (2021)), YOLOF(Chen et al. (2021)), and YOLOX(Ge et al. (2021)). These algorithms introduced a wealth of innovative ideas and development paths for advancing one-stage object detection.

The defects in synthetic leather can be primarily categorized into two major types: linear defects, including scratches, creases, fine stripes, etc., and point defects, such as white spots, black spots, stains, insect marks, oil stains, impurities, particles, burns, etc. Since detection of large-sized defects is relatively straightforward, this paper focuses solely on the more challenging task of detecting small-sized defects with deep learning algorithms. Specif-

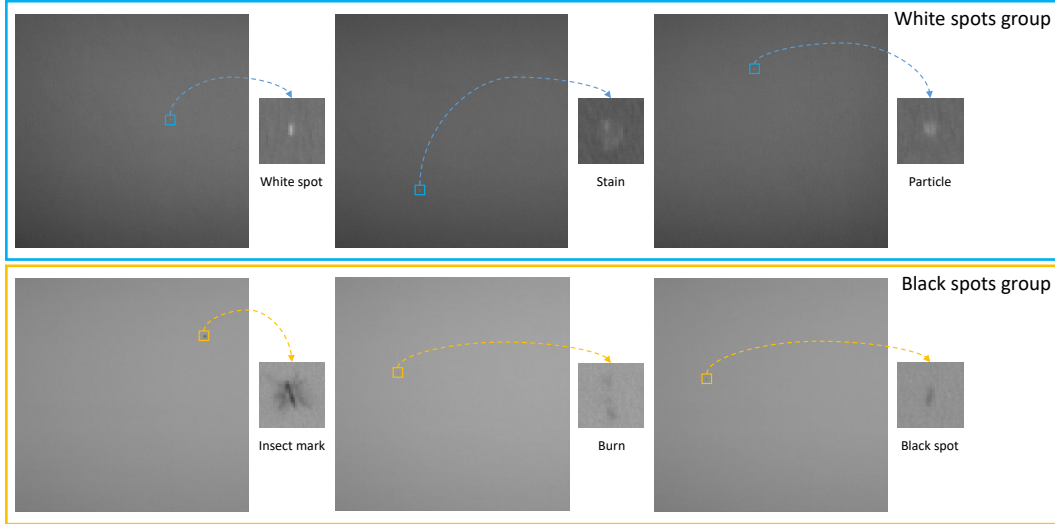


Figure 2: Two types of artificial leather defects are black spots and white spots.

ically, the defects of interest include black spots, white spots, insect marks, impurities, particles, burns, and stains. These defects, when imaged using illumination and industrial grayscale cameras, can be broadly categorized into two groups: black spots and white spots (Fig.2). The baseline model adopted in this paper is YOLOv5(Glenn (2021)). Due to the relatively small size of the defects in synthetic leather (ranging from 4 pixels to 20 pixels), the structure of YOLOv5 is requires careful adaption. The neck structure of YOLOv5 consists of a feature pyramid network (FPN)(Kim et al. (2018)) and a path aggregation network (PAN)(Liu et al. (2018)). However, this design leads to inconsistent neck depths for detection heads of different scales, particularly for the detection of small-sized object(Liu et al. (2021)) head. Consequently, YOLOv5 exhibits relatively lower average precision (AP) for small object detection. To address this issue and leverage the characteristics of synthetic leather defects, this paper proposes a novel double feature pool object detector, named "YOLOD".

This paper begins by evaluating the model on the public dataset MS-COCO(Lin et al. (2014)), where YOLOD demonstrates an average precision (AP)(Lin et al. (2014)) improvement ranging from **0.4%** to **2.6%** over YOLOv5. Additionally, as YOLOv5 does not report small object average precision (AP_S)(Lin et al. (2014)), this study performs a comparative analysis of YOLOD's small object detection AP_S with that of YOLOX(Ge et al.

(2021)) and YOLOv4-CSP(Bochkovskiy et al. (2020)), which shows a noticeable increases from **2.5%** to **4.1%**, respectively. Moreover, this paper evaluates the model on the Artificial leather dataset collected from a real industry project. In this evaluation, YOLOD exhibits an impressive **11.7%** - **13.5%** increase in AP_{50} compared to YOLOv5, along with a significant **5.2%** - **7.2%** reduction in the error detection rate. In summary, the contributions of this paper can be outlined as follows:

1. This paper proposes a novel neck network called the "dual feature pool" to effectively tackle the challenge of small object detection caused by imbalanced depth within the neck network, built upon the FPN+PAN structure. The dual feature pool structure not only addresses the issue and enhances the AP_S , but also leads to an overall improvement of the AP. Additionally, the proposed model demonstrates enhanced detection capabilities of small defects in artificial leather.

2. This paper proposes a novel structure called the "Interference Feature Filtering." This structure assesses the quality of channel feature maps at critical nodes and effectively filters out 0.5% to 5% of the low-score channel feature maps. This approach effectively reduces the interference of irregular patterns in artificial leather on small defects during the feature decomposition process.

3. This paper has enhanced the technique for incorporating positive samples in the loss function. This improvement facilitates the automatic expansion of the number of positive samples based on the bounding box size of the ground truth.

4. This paper thoroughly analyzed the method of eliminating grid sensitivity (Yolo4Bochkovskiy et al. (2020)). Subsequently, we propose an enhanced approach that involves modifying the slope of the sigmoid curve to achieve better convergence when increasing the scale parameter.

2. Dataset

2.1. Microsoft coco: Common objects in context (MS-COCO)

Since YOLOv4, one-stage object detection has been evaluated using MS-COCO dataset. YOLOD is also evaluated using the MS-COCO dataset. The training set of MS-COCO train2017 dataset consists of 118,287 images along with corresponding object annotation. The validating set of MS-COCO val2017 dataset contains 5,000 images and corresponding object annotation

Table 1: The performance metrics for evaluating object detection on the MSCOCO dataset

Metrics	Description
Average Precision (AP):	
AP	AP at IoU=.50:.05:.95 (primary challenge metric)
$AP^{IoU=.50}$	AP at IoU=.50 (PASCAL VOC metric)
$AP^{IoU=.75}$	AP at IoU=.75 (strict metric)
AP Across Scales:	
AP^{small}	AP for small objects: area $<32^2$
AP^{medium}	AP for medium objects: $32^2 < \text{area} < 96^2$
AP^{large}	AP for large objects: area $>96^2$
Average Recall (AR):	
$AR^{max=1}$	AR given 1 detection per image
$AR^{max=10}$	AR given 10 detections per image
$AR^{max=100}$	AR given 100 detections per image
AR Across Scales:	
AR^{small}	AR for small objects: area $<32^2$
AR^{medium}	AR for medium objects: $32^2 < \text{area} < 96^2$
AR^{large}	AR for large objects: area $>96^2$

data, which are mainly utilized for model evaluation. Furthermore, the MSCOCO test2017 dataset includes 40,670 images without corresponding object annotation data, for testing. To evaluate the performance on this dataset, the inference results (JSON(Pezoa et al. (2016)) format data) are required to be uploaded to the official MS-COCO website¹ for evaluation, which are assessed using a number of matrices presented in Tab.1.

2.2. Artificial leather dataset (ALD)

The defect dataset of Artificial leather originates from a real project conducted by our company. In the initial data collection phase, we employed a proof-of-concept (POC) device comprising an led, camera, control software, mechanical structure, and computing equipment. The ALD train2021 dataset consists of 10,000 images for model training, and 2,000 images for model evaluation. Furthermore, this paper introduces one new metric for

¹<https://cocodataset.org/>

Table 2: The performance metrics for evaluating object detection on the MSCOCO dataset

Metrics		Results	
		Positive	Negative
Ground-truth	True	TP	FN
	False	FP	TN

evaluating the model, which is based on the dataset’s unique characteristics and the standard evaluation metrics(Tab.2). The calculation process of the standard evaluation metrics is as follows:

$$Precision = \frac{TP}{TP + FP} \cdot 100\% \tag{1}$$

$$Recall = \frac{TP}{TP + FN} \cdot 100\% \tag{2}$$

The calculation process of the newly evaluation metric in this paper is as follows:

$$ErrorDetection = \frac{FP}{FP + TP} \cdot 100\% \tag{3}$$

In this paper, the prioritization of the AP₅₀ metric for model evaluation on the ALD dataset is emphasized, along with the inclusion of the error detection rate(Formula.3, The average error detection rate for the classification is denoted as AE) metric to assess the model’s ability to discern non-defect features. Given that the interference from irregular dermatoglyphics of Artificial leather often results in numerous false positives by the model, significantly impacting actual production, we have introduced this metric. This particular metric primarily calculates the proportion of false positives (FP) in the judgment results to the total number of determined defects.

3. YOLOD

3.1. Dual Feature Pool

An analysis of the FPN(Kim et al. (2018)) + PAN(Liu et al. (2018)) structure was conducted before proposing the new structure. It was found that in this combined architecture, the detection network’s depth for small objects is

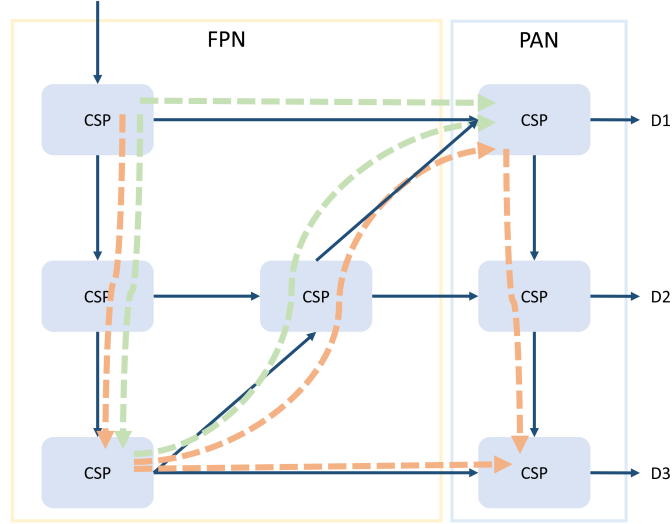


Figure 3: The FPN+PAN structure. The orange dashed arrow represents the network path of the detection head D3, while the green dashed arrow represents the network path of the detection head D1. It is evident that the orange network is deeper than the green network. Partial convolution and SPP(He et al. (2015)) are not included from the figure.

shallower than that of the network for detecting large objects (Fig. 3). To improve network detection accuracy, increasing the depth and width of the network becomes essential(Tan and Le (2019)). Consequently, the FPN+PAN structure was sub-optimal for the detection of small objects. To address this problem, the objective was to discover a structure that could enhance the depth or width of the small object detection network, thereby improving the accuracy of detecting small objects. Consequently, the dual feature pool structure (DFP) was developed. In this context, the terminology is defined as follows: the features directly output from the backbone network are referred to as "source features," and the features processed by the neck network are termed "processed features."

The network structure is divided into three parts. The first part adopts a structure similar to CSPNetWang et al. (2020), which divides three-level source features outputted by the backbone network into two parts through convolution using a half-channel. In the second part, one of the two outputs from each level is fused to form two feature pools (Fig. 4). The third part fuses another portion of the source features outputted at different levels with the output of the two feature pools. Before inputting each detection head,

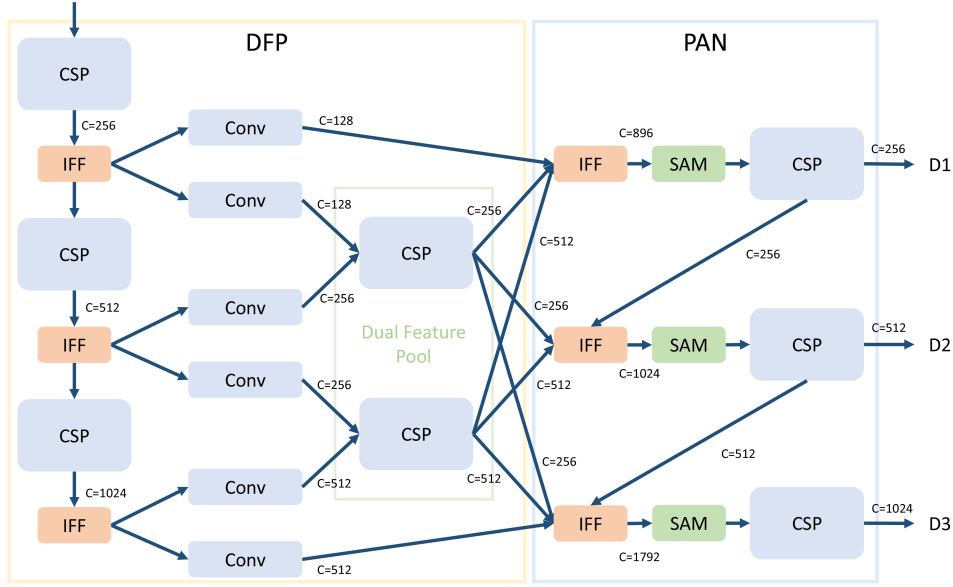


Figure 4: The diagram illustrates the DFP+PAN structure. The green box contains two CSP(Wang et al. (2020)) structures formed by the combination of three-level features. These two CSP structures constitute two feature pools of different scales and output features to the detection head. Partial convolution and SPP are excluded from the figure.

the fused features are enhanced using Interference Feature Filtering (IFF) and Spatial Attention Module(SAM)(Woo et al. (2018)). By employing this structure, the goal was to expand the network width as much as possible while keeping the network depth unchanged. The DFP structure is comprised of these three parts, which effectively widens the entire neck section, particularly the small object detection network. The two feature pools play a crucial role as they integrate small-medium-scale and medium-large-scale features, offering more feature dimensions to the detection head. Following the fusion in the third part, the dimension of features passed to the detection head increases by 1.75 to 2 times compared to FPN + PAN. The initial intention behind adopting this structure was to expand the width of the small object network.

3.2. Interference Feature Filtering

The quality of the feature maps produced by the convolutional network during the feature extraction process can be variable. Such variability may impact the effectiveness of deeper convolutional networks. To address this

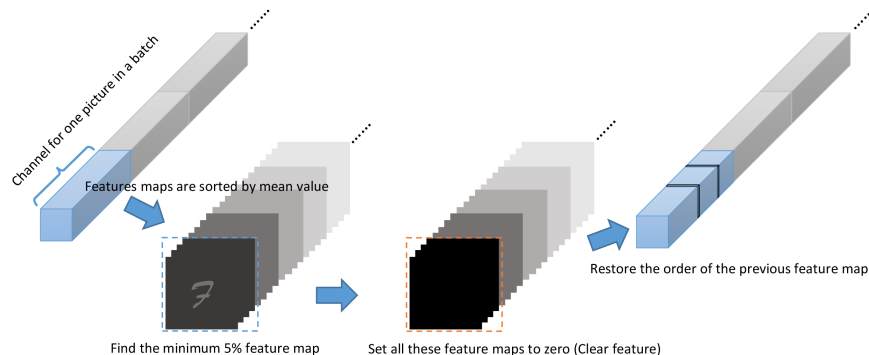


Figure 5: Interference feature filtering process.

issue, we devised a module that scores each channel’s feature map based on its mean value. Subsequently, we removed channel features with lower scores, where the removal ratios ranged from 0.5% to 5%(Fig. 5). The proposed structure focuses on two key aspects: the output of the backbone network and the concatenation of source features and processed features (Fig. 4). IFF is applied to the source feature output of the backbone network to ensure the purity of the features provided to the neck(Bochkovskiy et al. (2020)). The belief is that the quality of source features directly impacts the quality of the processed features, which, in turn, affects the accuracy of detection.

Additionally, IFF is utilized at the concatenation of source features and processed features because the number of feature channels after concatenation is significantly larger than the number of channels that ultimately pass through CSP. The intention is to reduce low-quality features for large-scale channel compression, thereby enhancing the quality of the features output after channel compression. The percentage of filtered features decreases linearly from 5% to 0.5% during the training process, as the interference features decrease. It is worth noting that if too many features are filtered, it may lead to a decrease in detection accuracy.

3.3. Adaptive Multi Positives

Both YOLOv5(Glenn (2021)) and YOLOX(Ge et al. (2021)) proposed different methods to increase the number of positive samples. YOLOv5 selects one or two positive samples from the top, bottom, left, and right grids based on the offset of the ground truth’s center point, resulting in a total of two or three positive samples. YOLOX considers the grid around the center point

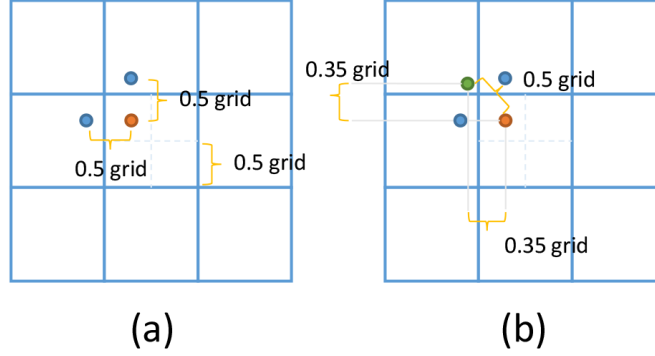


Figure 6: Panel (a) illustrates the YOLOv5 method of adding positive samples, while panel (b) presents our method of adding positive samples. In panel (b), the positive sample (green dot) was added in the upper-left corner. The Euclidean distance from the new positive sample to the center of the ground truth is 0.5 grid, the same as that used by YOLOv5 to expand the positive sample.

of the ground truth as positive samples. Our proposed Adaptive Multi Positives (AMP) method is an improvement of the YOLOv5’s approach (Fig. 6 (a)). The method of adding positive samples (Glenn (2021)) in Fig. 6 (b) represents the first step of our proposed method. If the offset of the ground truth is greater than or equal to 0.35 grid, the positive samples in the upper left corner will not be added. With the exception of the part shown in the figure, the expansion principle for the upper right, lower right, and lower left grids remains the same, calculated based on the offset of the ground truth’s center point. For instance, when the x-axis offset of the ground truth’s center point is greater than 0.65 grid and the y-axis offset is less than 0.35 grid (the value of 0.35 is calculated using the Euclidean distance formula with the assumption that the X coordinate is equal to the Y coordinate, and the Euclidean distance is 0.5), the positive sample in the upper right corner is added. The calculation process is summarized as follows:

$$P_{lt}^0 = \{(x, y), (x - 0.5, y), (x, y - 0.5), (x - 0.35, y - 0.35) \mid 0 \leq x < 0.35 \cap 0 \leq y < 0.35\} \quad (4)$$

$$P_{lt}^1 = \{(x, y), (x - 0.5, y), (x, y - 0.5) \mid 0.35 \leq x < 0.5 \cap 0.35 \leq y < 0.5\} \quad (5)$$

$$P_{rt}^0 = \{(x, y), (x + 0.5, y), (x, y - 0.5), (x + 0.35, y - 0.35) \mid 0.65 \leq x < 1 \cap 0 \leq y < 0.35\} \quad (6)$$

$$P_{rt}^1 = \{(x, y), (x - 0.5, y), (x, y - 0.5) | 0.5 \leq x < 0.65 \cap 0.35 \leq y < 0.5\} \quad (7)$$

$$P_{lb}^0 = \{(x, y), (x - 0.5, y), (x, y + 0.5), (x - 0.35, y + 0.35) | \\ 0 \leq x < 0.35 \cap 0.65 \leq y < 1\} \quad (8)$$

$$P_{lb}^1 = \{(x, y), (x - 0.5, y), (x, y + 0.5) | 0.35 \leq x < 0.5 \cap 0.5 \leq y < 0.65\} \quad (9)$$

$$P_{rb}^0 = \{(x, y), (x + 0.5, y), (x, y + 0.5), (x + 0.35, y + 0.35) | \\ 0.65 \leq x < 1 \cap 0.65 \leq y < 1\} \quad (10)$$

$$P_{rb}^1 = \{(x, y), (x - 0.5, y), (x, y + 0.5) | 0.5 \leq x < 0.65 \cap 0.5 \leq y < 0.65\} \quad (11)$$

where p^0 denotes the positive sample set augmented by AMP, and p^1 identifies the positive sample set of YOLOv5. P_{lt} , P_{lb} , P_{rt} , and P_{rb} represent the sets of positive samples in the four directions near the center grid of the ground truth (gt) point, and $x \in [0, 1]$ and $y \in [0, 1]$.

An additional step in our approach automatically selects and augments the count of positive samples based on the dimensions of the ground truth bounding box. No positive samples are added if the ground truth bounding box size is smaller than one grid. When the ground truth bounding box size is equal to or exceeds one grid, we follow the approach employed by YOLOv5 to increase positive samples. Furthermore, if the ground truth bounding box size is equal to or exceeds two grids, we employ our proposed method to add positive samples. We avoid adding positive samples when the number of grids encompassed by the ground truth bounding box is less than one, as these additional grids lack object features. Consequently, this precaution mitigates potential false detections and their adverse impact on the network’s ability to learn from the features present in the ground truth.

3.4. Eliminate Output Sensitivity

Since YOLOv4 introduced the elimination of grid sensitivity (Bochkovski et al. (2020)) (Eq.12), this approach has been adopted by many algorithms to mitigate the impact of grid squares in which objects are undetectable.

However, we have identified an issue: as the value of the scale parameter increases, the slope in the region near $t_{x,y}$ also increases (as illustrated in Fig.7(a)). Upon deriving the formula in Eq.12, we arrive at Eq.13. When $t_{x,y} = 0$, the slope is at its maximum, and the maximum slope is linked to the scale value. Consequently, increasing the scale value to eliminate grid sensitivity results in a very large slope near $t_{x,y} = 0$. An input value ($t_{x,y}$) near 0 can cause poor convergence of the network.

$$b_{x,y} = scale \cdot \sigma(t_{x,y}) - \frac{scale - 1}{2} + c_{x,y} \quad (12)$$

$$b'_{x,y} = \frac{scale \cdot e^{-t_{x,y}}}{(1 + e^{-t_{x,y}})^2} \quad (13)$$

$$b_{x,y} = scale \cdot \sigma\left(t_{x,y} \cdot \frac{\alpha}{scale}\right) - \frac{scale - 1}{2} + c_{x,y} \quad (14)$$

$$b'_{x,y} = \frac{\alpha \cdot e^{-t_{x,y} \frac{\alpha}{scale}}}{(1 + e^{-t_{x,y} \frac{\alpha}{scale}})^2} \quad (15)$$

An improvement was made to the previous method (Eq.14). $t_{x,y}$ is multiplied by a parameter, $\frac{\alpha}{scale}$, where α represents a fixed slope value. When the elimination of grid sensitivity used in YOLOv4 is considered as the benchmark, α takes the value 2. On the other hand, when not eliminating the grid sensitivity (as done in YOLOv3(Redmon and Farhadi (2018))), α is set to 1. By taking the derivative of Eq.14 (as shown in Eq. 15), it can be observed that the slope is related to α when $t_{x,y} = 0$. In this approach, we utilize a fixed value α instead of a variable value scale. As a result, when eliminating the sensitivity of the grid in this manner, the slope of the curve remains unchanged (as depicted in Fig. 7 (b)). In our experiment, we set α to 2.

4. Experiments(ALD)

This experiment utilizes the artificial leather dataset(ALD) to compare the detection capabilities of YOLOv4 and YOLOv5-r5.0² on artificial leather defects. The experimental model did not utilize any pre-trained model, and initialization parameters were randomly set. For fairness, all models were trained for only 300 epochs using mixed-precision training(Micikevicius

²<https://github.com/ultralytics/yolov5/releases/tag/v5.0>

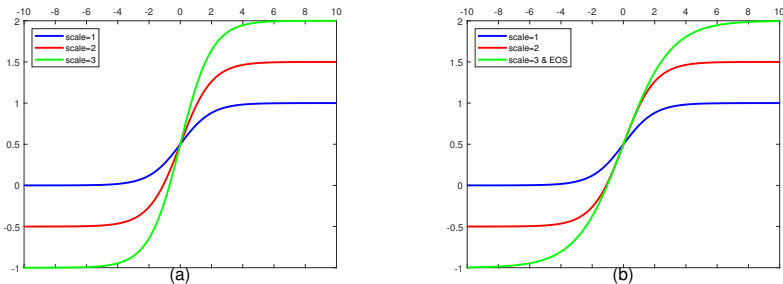


Figure 7: Figure (a) shows the sigmoid function curve when scale takes different values, and figure (b) shows the sigmoid function curve when scale = 3 and EOS is added.

Table 3: Comparison of YOLOD and YOLOv5 in terms of AP on ALD. All the models are tested at 640*640 resolution, with FP16-precision and batch=1 on a RTX3090

Models	AP ₅₀	AE	Parameters(M)	GFLOPs	Latency(ms)
YOLOv5-S	64.4	20.8	7.3	17.1	8.7
YOLOD-S	77.9(+13.5)	15.6(-5.2)	10.6	22.9	11.2
YOLOv5-M	78.5	14.4	21.4	51.4	11.1
YOLOD-M	90.7(+12.2)	7.8(-6.6)	26.6	58.7	16.2
YOLOv5-L	84.6	10.4	47.1	115.6	13.7
YOLOD-L	96.3(+11.7)	3.2(-7.2)	52.1	118.1	21.2

et al. (2017)). Since all defects in the artificial leather dataset are single-channel gray images, conventional data augmentation methods such as mosaic(Bochkovskiy et al. (2020)), mixup(Zhang et al. (2017)), and copy-paste(Ghiasi et al. (2021)) were not used in the experiment. To ensure comparability with previous models, all hyperparameters³, Backbone, SiLU activation, and Cosine annealing scheduler(Loshchilov and Hutter (2016)) were kept consistent with those of YOLOv5-r5.0. All experiments were conducted on a single graphics card (RTX3090).

Through comparative experiments (Tab.3), YOLOD’s AP₅₀ is significantly higher than YOLOv5, with a difference of 11.7% - 13.5%. This data indicates that YOLOD has a much better detection capability for artificial

³<https://github.com/ultralytics/yolov5/blob/master/data/hyps/hyp.scratch-high.yaml>

Table 4: Ablation Experiment on MS-COCO val2017

IFF	AMP	EOS	DFP	AP(%)	AP_{50}	AP_{75}	AP_S	AP_M	AP_L
				48.2	66.9	-	-	-	-
✓				48.3(+0.1)	66.9	52.0	30.9	53.2	62.6
✓	✓			48.3	66.9	52.2	31.2	53.3	62.1
✓	✓	✓		48.5(+0.2)	67.1	52.7	31.2	53.5	62.4
✓	✓	✓	✓	48.6(+0.1)	67.2	52.9	32.3	53.7	62.5

leather defects compared to YOLOv5. Additionally, YOLOD’s AE data is 5.2% - 7.2% lower than YOLOv5, which demonstrates that YOLOD has a much better error detection capability for artificial leather defects than YOLOv5. In practical projects, customers also pay more attention to these two metrics. Therefore, these two metrics fully illustrate that YOLOD outperforms YOLOv5 in terms of artificial leather defect detection performance.

5. Experiments(MS-COCO)

The experiment employed MS-COCO 2017(Lin et al. (2014)) dataset for verifying YOLOD, using YOLOv5-r5.0 data as the baseline. The experimental model did not utilize any pre-trained model, and initialization parameters were randomly set. For fairness, all models were trained for only 300 epochs using mixed-precision training. During training, data augmentation methods, such as mosaic, mixup, and copy-paste, were applied. To ensure comparability with previous models, all hyperparameters, Backbone, SiLU activation, Cosine annealing scheduler, and data augmentation methods were kept consistent with those of YOLOv5, except for using a smaller learning rate. Mosaic, mixup, and copy-paste were removed during training up to the 286th epoch, and all data augmentation was removed during training up to the 296th epoch. All experiments were conducted on a single graphics card (RTX3090).

5.1. Ablation Experiment

The experiment primarily compared the innovations’ data on MS-COCO val2017. We assessed the impact of adding DFP, IFF, AMP, and EOS on the model’s average precision (AP) and particularly focused on the AP of small objects (Table. 4). It was observed that only DFP and AMP showed

Table 5: Comparison of YOLOv4, YOLO-X and YOLOv4-CSP in terms of AP_S on MS-COCO.

Models	Size	AP_S	AP_M	AP_L
YOLOv4-CSP	640	28.2	51.2	59.8
YOLO-X-L	640	29.8	54.5	64.4
YOLOv4-L	640	32.3(+2.5)	53.7	62.1

improvements over the baseline. Regarding IFF, the analysis indicated that too many effective features might have been filtered out, and the location of IFF also had an impact. To address this, we plan to readjust the filtering proportion, consider an adaptive way to adjust the filtering proportion of IFF, or design a more rational method to distinguish interference features. Nevertheless, IFF exhibited outstanding performance in both M-size and S-size models in the experiment. As for EOS, we hypothesize that the reason for its lack of improvement could be the input being multiplied by a variable ($\frac{\alpha}{scale}$) less than 1 to increase its range, resulting in increased learning costs for the network.

5.2. Comparative experiment

After adding DFP, the model’s average precision (AP) exceeded that of YOLOv5, and there was a significant increase in the AP for small objects. For a more detailed comparison, we separately analyzed the AP of small objects; however, YOLOv5 only provides data for AP and AP_{50} . Consequently, we compared the data with YOLOv4-CSP and YOLOX, both having similar model sizes and the same input resolution. Our model outperformed the other models in terms of detection AP for small objects (Table. 5).

In the experiment, we used three model sizes: large (L), medium (M), and small (S), for comparison with YOLOv5. The comparison data included AP, parameters, GFLOPs, and latency (Table. 6). Taking the L-size model as the benchmark, we scaled the depth and width of our M model by multiplying the depth by 0.67, which represents the number of residual blocks(He et al. (2016)) in CSP, and the width by 0.75, which represents the number of channels. For the S model, the depth was multiplied by 0.3, and the width was multiplied by 0.5. Our model achieved 0.4%–2.6% higher AP than YOLOv5, with a minimal difference in parameters and GFLOPs.

Table 6: Comparison of YOLOD and YOLOv5 in terms of AP on MS-COCO. All the models are tested at 640*640 resolution, with FP16-precision and batch=1 on a RTX3090

Models	AP(%)	Parameters(M)	GFLOPs	Latency(ms)
YOLOv5-S	36.7	7.3	17.1	8.7
YOLOD-S	39.3(+2.6)	10.6	22.9	11.2
YOLOv5-M	44.5	21.4	51.4	11.1
YOLOD-M	45.6(+1.1)	26.6	58.7	16.2
YOLOv5-L	48.2	47.1	115.6	13.7
YOLOD-L	48.6(+0.4)	52.1	118.1	21.2

5.3. Comparison with SOTA

Finally, the experiment was compared with other state-of-the-art (SOTA) data (Table. 7). As access to a Tesla V100 graphics card was unavailable, the model’s calculation speed depended on hardware and software, beyond our control. Therefore, FPS calculations were conducted using the available RTX3090 graphics cards, and FPS was calculated without considering the time taken for post-processing and NMS.

Upon comparing the model with other SOTA approaches, it was observed that the calculation speed was close to that of YOLOv5, while the model’s accuracy had been improved to a certain extent. Notably, the detection accuracy of the model for small objects exceeded that of the other models.

6. Conclusion

In this study, four effective innovation modules were proposed for the structure of the YOLOv5 model, combined with the defect characteristics of artificial leather, forming a new algorithm called YOLOD. YOLOD achieves a higher AP(0.4% - 2.6%) than YOLOv5 on the general MS-COCO dataset, with minimal impact on the inference speed. Additionally, YOLOD exhibits better AP (+11.7% to +13.5%) and lower AE (-5.2% to -7.2%) than YOLOv5 on the artificial leather defect dataset. As small object detection has always been a challenging task for YOLO series algorithms, the method proposed in this paper effectively solves the problem of small object detection, leading to improved AP. Moreover, it performs well in detecting small defects in artificial leather, providing a useful reference for other researchers in applying YOLO series models more effectively.

Table 7: Comparison of the speed and accuracy of different object detectors on MS-COCO 2017 test-dev. We select all the models trained on 300 epochs for fair comparison.

Method	Size	FPS	AP(%)	AP_{50}	AP_{75}	AP_S	AP_M	AP_L
RetinaNet	640	37	37	-	-	-	-	-
RetinaNet	640	29.4	37.9	-	-	-	-	-
RetinaNet	1024	19.6	40.1	-	-	-	-	-
RetinaNet	1024	15.4	41.1	-	-	-	-	-
YOLOv3 + ASFF*	320	60	38.1	57.4	42.1	16.1	41.6	53.6
YOLOv3 + ASFF*	416	54	40.6	60.6	45.1	20.3	44.2	54.1
YOLOv3 + ASFF*	608×	45.5	42.4	63.0	47.4	25.5	45.7	52.3
YOLOv3 + ASFF*	800×	29.4	43.9	64.1	49.2	27.0	46.6	53.4
EfficientDet-D0	512	62.5	33.8	52.2	35.8	12.0	38.3	51.2
EfficientDet-D1	640	50.0	39.6	58.6	42.3	17.9	44.3	56.0
EfficientDet-D2	768	41.7	43.0	62.3	46.2	22.5	47.0	58.4
EfficientDet-D3	896	23.8	45.8	65.0	49.3	26.6	49.4	59.8
PP-YOLOv2	640	68.9	49.5	68.2	54.4	30.7	52.9	61.2
PP-YOLOv2	640	50.3	50.3	69.0	55.3	31.6	53.9	62.4
YOLOv4	608	62.0	43.5	65.7	47.3	26.7	46.7	53.3
YOLOv4-CSP	640	73.0	47.5	66.2	51.7	28.2	51.2	59.8
YOLOX-M	640	81.3	46.4	65.4	50.6	26.3	51.0	59.9
YOLOX-L	640	69.0	50.0	68.5	54.5	29.8	54.5	64.4
YOLOX-X	640	57.8	51.2	69.6	55.7	31.2	56.1	66.1
YOLOv3-ultralytics	640	95.2	44.3	64.6	-	-	-	-
YOLOv5-S	640	114.9	36.7	55.4	-	-	-	-
YOLOv5-M	640	90.1	44.5	63.1	-	-	-	-
YOLOv5-L	640	73.0	48.2	66.9	-	-	-	-
YOLOv5-X	640	62.5	50.4	68.8	-	-	-	-
YOLOD-S	640	89.2	39.3	56.6	42.6	22.1	44.2	51.8
YOLOD-M	640	61.7	45.6	63.5	49.5	29.1	50.4	59.4
YOLOD-L	640	47.2	48.6	66.7	52.7	32.3	53.7	62.1

7. Acknowledge

This work was supported by the National Natural Science Foundation of China [Nos. 61972060, U1713213 and 62027827], National Key Research and Development Program of China (Nos. 2019YFE0110800), Natural Science Foundation of Chongqing [cstc2020jcyj-zdxmX0025, cstc2019cxcyljrc-td0270].

References

- Bochkovskiy, A., Wang, C.Y., Liao, H.Y.M., 2020. Yolov4: Optimal speed and accuracy of object detection. arXiv preprint arXiv:2004.10934 .
- Cai, Z., Vasconcelos, N., 2018. Cascade r-cnn: Delving into high quality object detection, in: Proceedings of the IEEE conference on computer vision and pattern recognition, pp. 6154–6162.
- Cao, Z., Liao, T., Song, W., Chen, Z., Li, C., 2021. Detecting the shuttlecock for a badminton robot: A yolo based approach. Expert Systems with Applications 164, 113833.
- Chen, Q., Wang, Y., Yang, T., Zhang, X., Cheng, J., Sun, J., 2021. You only look one-level feature, in: Proceedings of the IEEE/CVF conference on computer vision and pattern recognition, pp. 13039–13048.
- Dai, J., Li, Y., He, K., Sun, J., 2016. R-fcn: Object detection via region-based fully convolutional networks. Advances in neural information processing systems 29.
- Ge, Z., Liu, S., Wang, F., Li, Z., Sun, J., 2021. Yolox: Exceeding yolo series in 2021. arXiv preprint arXiv:2107.08430 .
- Ghiasi, G., Cui, Y., Srinivas, A., Qian, R., Lin, T.Y., Cubuk, E.D., Le, Q.V., Zoph, B., 2021. Simple copy-paste is a strong data augmentation method for instance segmentation, in: Proceedings of the IEEE/CVF conference on computer vision and pattern recognition, pp. 2918–2928.
- Girshick, R., 2015. Fast r-cnn, in: Proceedings of the IEEE international conference on computer vision, pp. 1440–1448.

- Girshick, R., Donahue, J., Darrell, T., Malik, J., 2014. Rich feature hierarchies for accurate object detection and semantic segmentation, in: Proceedings of the IEEE conference on computer vision and pattern recognition, pp. 580–587.
- Glenn, J.e.a., 2021. Yolov5. <https://github.com/ultralytics/yolov5>.
- He, K., Gkioxari, G., Dollár, P., Girshick, R., 2017. Mask r-cnn, in: Proceedings of the IEEE international conference on computer vision, pp. 2961–2969.
- He, K., Zhang, X., Ren, S., Sun, J., 2015. Spatial pyramid pooling in deep convolutional networks for visual recognition. *IEEE transactions on pattern analysis and machine intelligence* 37, 1904–1916.
- He, K., Zhang, X., Ren, S., Sun, J., 2016. Deep residual learning for image recognition, in: Proceedings of the IEEE conference on computer vision and pattern recognition, pp. 770–778.
- Huang, X., Wang, X., Lv, W., Bai, X., Long, X., Deng, K., Dang, Q., Han, S., Liu, Q., Hu, X., et al., 2021. Pp-yolov2: A practical object detector. arXiv preprint arXiv:2104.10419 .
- Karaman, A., Pacal, I., Basturk, A., Akay, B., Nalbantoglu, U., Coskun, S., Sahin, O., Karaboga, D., 2023. Robust real-time polyp detection system design based on yolo algorithms by optimizing activation functions and hyper-parameters with artificial bee colony (abc). *Expert Systems with Applications* 221, 119741.
- Kim, S.W., Kook, H.K., Sun, J.Y., Kang, M.C., Ko, S.J., 2018. Parallel feature pyramid network for object detection, in: Proceedings of the European conference on computer vision (ECCV), pp. 234–250.
- Lin, T.Y., Goyal, P., Girshick, R., He, K., Dollár, P., 2017. Focal loss for dense object detection, in: Proceedings of the IEEE international conference on computer vision, pp. 2980–2988.
- Lin, T.Y., Maire, M., Belongie, S., Hays, J., Perona, P., Ramanan, D., Dollár, P., Zitnick, C.L., 2014. Microsoft coco: Common objects in context, in: *Computer Vision–ECCV 2014: 13th European Conference, Zurich*,

- Switzerland, September 6-12, 2014, Proceedings, Part V 13, Springer. pp. 740–755.
- Liu, S., Huang, D., Wang, Y., 2019. Learning spatial fusion for single-shot object detection. arXiv preprint arXiv:1911.09516 .
- Liu, S., Qi, L., Qin, H., Shi, J., Jia, J., 2018. Path aggregation network for instance segmentation, in: Proceedings of the IEEE conference on computer vision and pattern recognition, pp. 8759–8768.
- Liu, W., Anguelov, D., Erhan, D., Szegedy, C., Reed, S., Fu, C.Y., Berg, A.C., 2016. Ssd: Single shot multibox detector, in: Computer Vision–ECCV 2016: 14th European Conference, Amsterdam, The Netherlands, October 11–14, 2016, Proceedings, Part I 14, Springer. pp. 21–37.
- Liu, Y., Sun, P., Wergeles, N., Shang, Y., 2021. A survey and performance evaluation of deep learning methods for small object detection. *Expert Systems with Applications* 172, 114602.
- Long, X., Deng, K., Wang, G., Zhang, Y., Dang, Q., Gao, Y., Shen, H., Ren, J., Han, S., Ding, E., et al., 2020. Pp-yolo: An effective and efficient implementation of object detector. arXiv preprint arXiv:2007.12099 .
- Loshchilov, I., Hutter, F., 2016. Sgdr: Stochastic gradient descent with warm restarts. arXiv preprint arXiv:1608.03983 .
- Micikevicius, P., Narang, S., Alben, J., Diamos, G., Elsen, E., Garcia, D., Ginsburg, B., Houston, M., Kuchaiev, O., Venkatesh, G., et al., 2017. Mixed precision training. arXiv preprint arXiv:1710.03740 .
- Pang, J., Chen, K., Shi, J., Feng, H., Ouyang, W., Lin, D., 2019. Libra r-cnn: Towards balanced learning for object detection, in: Proceedings of the IEEE/CVF conference on computer vision and pattern recognition, pp. 821–830.
- Pezoa, F., Reutter, J.L., Suarez, F., Ugarte, M., Vrgoč, D., 2016. Foundations of json schema, in: Proceedings of the 25th international conference on World Wide Web, pp. 263–273.
- Pourkaramdel, Z., Fekri-Ershad, S., Nanni, L., 2022. Fabric defect detection based on completed local quartet patterns and majority decision algorithm. *Expert Systems with Applications* 198, 116827.

- Redmon, J., Divvala, S., Girshick, R., Farhadi, A., 2016. You only look once: Unified, real-time object detection, in: Proceedings of the IEEE conference on computer vision and pattern recognition, pp. 779–788.
- Redmon, J., Farhadi, A., 2017. Yolo9000: better, faster, stronger, in: Proceedings of the IEEE conference on computer vision and pattern recognition, pp. 7263–7271.
- Redmon, J., Farhadi, A., 2018. Yolov3: An incremental improvement. arXiv preprint arXiv:1804.02767 .
- Ren, S., He, K., Girshick, R., Sun, J., 2015. Faster r-cnn: Towards real-time object detection with region proposal networks. Advances in neural information processing systems 28.
- Tan, M., Le, Q., 2019. Efficientnet: Rethinking model scaling for convolutional neural networks, in: International conference on machine learning, PMLR. pp. 6105–6114.
- Tan, M., Pang, R., Le, Q.V., 2020. Efficientdet: Scalable and efficient object detection, in: Proceedings of the IEEE/CVF conference on computer vision and pattern recognition, pp. 10781–10790.
- Wang, C.Y., Bochkovskiy, A., Liao, H.Y.M., 2021. Scaled-yolov4: Scaling cross stage partial network, in: Proceedings of the IEEE/cvf conference on computer vision and pattern recognition, pp. 13029–13038.
- Wang, C.Y., Bochkovskiy, A., Liao, H.Y.M., 2022. Yolov7: Trainable bag-of-freebies sets new state-of-the-art for real-time object detectors. arXiv preprint arXiv:2207.02696 .
- Wang, C.Y., Liao, H.Y.M., Wu, Y.H., Chen, P.Y., Hsieh, J.W., Yeh, I.H., 2020. Cspnet: A new backbone that can enhance learning capability of cnn, in: Proceedings of the IEEE/CVF conference on computer vision and pattern recognition workshops, pp. 390–391.
- Woo, S., Park, J., Lee, J.Y., Kweon, I.S., 2018. Cbam: Convolutional block attention module, in: Proceedings of the European conference on computer vision (ECCV), pp. 3–19.
- Zhang, H., Cisse, M., Dauphin, Y.N., Lopez-Paz, D., 2017. mixup: Beyond empirical risk minimization. arXiv preprint arXiv:1710.09412 .